

Jordan Meridith Hood

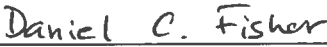
**Analysis of differential X-ray attenuation as a method for correlating
annual dentin increments in proboscidean tusks**

submitted in partial fulfillment of the requirements for the degree of
Master of Science in Earth and Environmental Sciences
Department of Earth and Environmental Sciences
The University of Michigan




Signature


Accepted by:




Name



Date



Signature




Name



Date



Department Chair Signature



Name



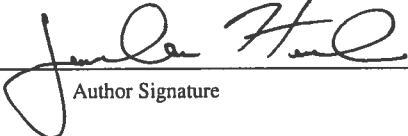
Date

I hereby grant the University of Michigan, its heirs and assigns, the non-exclusive right to reproduce and distribute single copies of my thesis, in whole or in part, in any format. I represent and warrant to the University of Michigan that the thesis is an original work, does not infringe or violate any rights of others, and that I make these grants as the sole owner of the rights to my thesis. I understand that I will not receive royalties for any reproduction of this thesis.

Permission granted.

Permission granted to copy after: _____

Permission declined.



Author Signature



Abstract

The tusks of woolly mammoths (*Mammuthus primigenius*) are composed of increments of dentin that form annually throughout an individual's entire life. Analyses of tusks, however, are frequently limited to study of discrete samples, often in the form of cores that each contain only a subset of the total number of years recorded in a tusk. These cores should be taken at locations that are close enough together to ensure that adjacent cores share some of the same years, and for a comprehensive analysis, a series of such cores should sample all the years in a tusk. A method for correlating annual increments between cores therefore plays a critical role in reconstructing the entire series of years contained in a tusk.

The density of tusk dentin is known to fluctuate annually. In this study, X-ray computed microtomography (microCT) scans of cores from the right tusk of the Yukagir mammoth show dramatic fluctuations of radiodensity associated with each year boundary. Mathematical correlation of these fluctuations (or density features) based on their unique pattern (or signature) of X-ray attenuation, expressed as luminance in three-dimensional reconstructions of microCT scans, is an effective way to correlate years between adjacent cores. The data described here demonstrate that correlation of density features between cores using attenuation signatures judged to be most similar (because they yielded the highest R-value when compared to candidate years in a neighboring core) supports the results of prior thin section analysis using daily and weekly increments to correlate years between cores. This study is a stringent test of this novel method of correlation as the Yukagir mammoth's tusk was previously sampled at locations relatively far apart, and its success suggests that this method can be used on many tusks for which coring is the only option for study.

Introduction

Proboscidean tusks grow continually throughout life and therefore allow for exploration of nearly the entire life history of an individual. Conceptually similar to studying tree growth rings, analyses of the number, density, isotopic composition, and thickness of layers of dentin within a tusk provide information about an individual such as age, nutritional status, calving cycles in a female, eviction from the matriarchal family unit in a male, and the season of death (Fisher, 1984, 1987, 1996, 2009, 2018; Fox and Fisher, 1994; Fisher and Fox, 2006, 2007). Tusks are valued not only by researchers but by museums as well, so it is difficult to obtain permission to study a tusk using destructive methods such as longitudinal sectioning, even though such methods allow direct visualization of all the dentin layers within a tusk.

Coring is a minimally destructive way to sample a tusk, and a series of cores can contain all of the layers of dentin created during the life of an individual if the cores are taken close enough together. Layers of dentin form a nested hierarchical system first described by Fisher (1987) in which annual layers, or increments, of dentin are punctuated by approximately weekly increments (in woolly mammoth tusks), which are in turn punctuated by daily increments (Koch et al., 1989; Fisher, 1996, 2001, 2009, 2018; Fisher and Fox, 2007). Since each core contains only a subset of consecutive annual increments of dentin within a tusk, a method is needed to correlate the few years that overlap between adjacent cores so that the entire series of years within a tusk can be reconstructed. Years are often correlated between cores by analyzing the thickness and number of weekly and daily increments within each year via microscopic analysis of thin sections and finding matching patterns of increments in adjacent cores (Fisher et al., 2010).

This study explores a novel method of correlating years between cores – using X-ray computed microtomography (microCT). Each annual dentin increment possesses variations in density throughout the year. MicroCT uses X-rays to measure the radiodensity of a material by quantifying the attenuation of X-ray beams (Racicot, 2016). Areas of higher radiodensity more greatly attenuate X-ray beams than areas of lower density, and are expressed as brighter voxels (the 3D-equivalent of pixels) in the resulting three-dimensional digital reconstruction of the material that was scanned. A general annual pattern of change in dentin density has previously been reported and is characterized by a sudden decrease in density at the onset of spring followed by a gradual increase in density throughout the rest of the year (Fisher et al., 2014; El Adli et al., 2015, 2017a, b; Cherney et al., 2017).

In this study, microCT scans of cores from the Yukagir mammoth show annually-occurring fluctuations in radiodensity that are more complex than previously described. The dentin around a winter-spring boundary (which marks the transition between two annual increments) contains more dramatic changes in radiodensity when compared to the rest of the year. However, not all years have exactly the same pattern, or signature, of radial variation in radiodensity. For example, one year may be characterized by two thin bands of high attenuation followed by an abrupt return to low attenuation, while another year may be characterized by one thick band of high attenuation followed by a gradual return to low attenuation. The dramatic fluctuations in radiodensity associated with year boundaries are referred to here as density features. This study investigates whether the signatures of annual density features seen in microCT scans are distinctive enough to allow for mathematical correlation of years between adjacent cores.

Materials and methods

Specimen

The Yukagir mammoth is an adult male woolly mammoth (*Mammuthus primigenius*) that lived during the late Pleistocene in what is now northern Yakutia (central Siberia), Russian Federation (Fisher, 2007). The mammoth's carcass was found in 2002, and is currently repositied in the collection of the Academy of Sciences of the Sakha Republic (Yakutia), in Yakutsk. Its tusks remain in reasonably good condition in part due to the specimen's preservation in permafrost. Both tusks have minimal breakage and are nearly complete, containing most of the annual increments of dentin formed during life.

Cores

The left tusk of the Yukagir mammoth remains within its alveolus while the right tusk was previously removed and sampled by drilling eleven cores, each 2 cm in diameter, along the length of the tusk at predetermined intervals (Figure 1) (Fisher, 2007; Fisher et al., 2010). The cores were drilled radially from the outer curve of the tusk, through the tusk's central axis, and out through the inner curve. Most cores were spaced 30 cm apart, a distance expected to be adequate for obtaining overlap of at least one year in adjacent cores, as the depth of the tusk pulp cavities of adult male woolly mammoths can be on the order of 45 cm (Figure 2a). Cores 1 and 2 were sampled 20 cm apart from each other, as were Cores 10 and 11, so that each of these pairs of adjacent cores contains some of the same annual increments of dentin, even though the pulp cavity may be shallower earlier and later in life than it is during the majority of adulthood (Smith and Fisher, 2011; 2013). This spacing strategy ensures that the series of eleven cores contains all

of the annual increments present in the tusk, and adjacent cores overlap slightly in the layers of dentin they contain, making correlation of years between cores possible.

The cores required some preparation before the annual increments within them could be studied. Since increments of dentin are conical in nature and the cores went all the way through the tusk, the years in each core are recorded twice, once on either side of the axis. The cores were cut transversely with the axis preferentially incorporated into the ventral half. The dorsal half of each core was left intact and stored for archival purposes. The ventral half of each core was cut into four slabs (using a diamond wafering blade 0.012” thick, producing minimal kerf-loss), with cuts oriented perpendicularly to the layers of dentin so that thin sections produced parallel to these cuts would reveal true increment thicknesses. The four slabs, consisting of the Proximal Heel (Slab 1), Slab 2, Slab 3, and the Distal Heel (Slab 4), were polished, and thin sections were made from the heels. Slabs 2 and 3 were each 5 mm thick, whereas heels were about 5 mm thick at their thickest point, tapering to a sharp edge. When viewed in a slab or thin section, an increment of dentin shared by two adjacent cores is represented nearer the tusk axis in the more distally located core and nearer the cementum in the more proximally located core (Figure 2b).

CT scans

The slabs made from the cores required mounting before microCT scanning could take place. Broken slab fragments were glued together using Paraloid B-72, chosen for its adhesive properties, archival quality, and reversibility with acetone (Cores 5 and 10 had broken during drilling, and Cores 9, 10, and 11 had broken into multiple pieces due to desiccation). Some heels had been cut into two pieces to fit onto standard petrographic microscope slides for the purpose of thin section analysis; these halves were glued together as well. The four slabs of each core

were glued onto a scaffold of wooden sticks attached to a sheet of cardboard. The slabs were arranged with the Proximal Heel on the left, followed by Slab 2 and Slab 3, and the Distal Heel on the right. The orientation of the cut surfaces was maintained. Each sheet was labeled with copper wire to record the specimen name and core number within the 3D reconstruction of the CT scans (e.g., the label “Y6” indicates the specimen name, “Y” for Yukagir mammoth, and the core number, “6” for the sixth core, counting in order from the tusk tip) (Figure 3). The sheet was trimmed prior to scanning to reduce file size, and slides containing thin sections made from the heels were removed from the sheet after a test scan revealed no information about the radiodensity of the dentin within them (because the attenuation of the glass slide was too great relative to the thin slice of dentin remaining on the slide). Each set of slabs was radiographically imaged using a Pinnacle X-ray Solutions Macro CT – 40/320, operating at 150 kV, 3.2 mA, and 500 ms, yielding uniform cubic voxels of 53 μm per side. A shot was taken every 0.25° of rotation, resulting in 1,440 shots per scan. Each sheet was oriented so that a single X-ray beam would not penetrate multiple slabs at once.

Data processing

The microCT scans were processed in Amira 6.0.1, software designed for 3D analysis. After a volume rendering was completed, the multi-planar viewer was used to visualize the material inside the slabs. Criteria such as lack of breakage and the absence of CT artifacts were used to determine which slab to analyze. Cores 9, 10, and 11 delaminated along multiple dentin layers due to desiccation and had to be excluded from this study because their features were too greatly obscured by this breakage. For all intact cores (Cores 1-8), Slab 3 was analyzed as opposed to the heels (Slabs 1 and 4) because the heels taper near the axis (Slab 1/Proximal Heel)

or near the cementum (Slab 4/Distal Heel) due to the angular relationship between the transverse cuts (perpendicular to dentin layers) and the core axes. As a result, Slabs 2 and 3 contain more material than the heels. The distal surface of Slab 3 was analyzed for each core because the proximal surface of Slab 3 and one or both surfaces of Slab 2 contain a small hole in the cementum left by the pilot bit, which served to stabilize the coring bit at the beginning of each coring operation. While this hole removed little to no dentin from each core, its presence did lead to artifacts in the 3D reconstruction of the CT data, which resulted in bright areas throughout the slab that did not accurately depict the density of the dentin.

The three planes of the multi-planar viewer (corresponding to virtual x-, y-, and z-axes) were oriented so that one plane ran parallel to the cut surface of the slab to maintain the perpendicularity of the plane to the layers of dentin in order to preserve their thicknesses. The histogram that controls the relation between attenuation and brightness of pixels (which represent 3D voxels) was adjusted to make the annually-occurring density features stand out. The features were most apparent when the thickness of the plane was set to 1.5 mm, which averaged the luminance of the voxels within 0.75 mm of the plane. The orientation and thickness of the plane resulted in a two-dimensional image of a slice through the slab that showed the annual density features of the dentin. Once a slice that showed the density features most prominently was selected, the length in millimeters of a physical edge of the slab was measured using the three-dimensional position coordinates given by Amira to confirm the scaling of the image. A snapshot of the selected slice was then taken and exported to ImageJ (Rasband, 1997), a program used for image analysis.

To set the scale in ImageJ, a transect was drawn along the same edge of the slab that was measured in Amira, yielding a scale in pixels per millimeter once the known distance was

entered. A radial transect was drawn from the outer surface of the slab (which was also the outer surface of the tusk) to the tusk axis, perpendicular to the density features, so that the transect ran from earlier-formed dentin to more recently-formed dentin. Due to the asymmetrical nature of the conical layers of dentin, occasionally no single radial transect maintained perpendicularity to all annual increments. In such cases, as with Cores 7 and 8, two slightly overlapping transects were drawn so that no layer of dentin would be unaccounted for. The two transects were later combined based on a landmark data point to yield a single series of data points spanning the entire slab. For each core, a graph of luminance (quantified as gray value) along the radial transect was created using the Plot Profile function in ImageJ.

Data analysis

Similar signatures of relative change in luminance (not similar values of attenuation) that characterize annual density features were used to correlate years between cores. Density features were not distinctive enough to match between cores based on visual inspection of either the slices of CT data or the graphs of luminance values. Each graph had a parabolic trend with higher values at the beginning and end of each transect, which was likely a result of beam hardening, a common artifact of CT reconstruction that brightens the edges of an object (Racicot, 2016), and did not accurately depict the density of the dentin in the slab (Figure 4). The density features near the beginning and end of each transect (near the cementum and tusk axis, respectively) were often obscured by these artificially high values. This is especially problematic because the features of interest (i.e., features associated with years that are shared between a pair of adjacent cores) are located nearer the axis in the more distally-located core and nearer the cementum in the more proximally-located core.

To make the density features more apparent, each graph was “detrended” to remove the overall parabolic shape. The portion of the graph of each transect that recorded the radiodensity of the cementum (in all cores except for Cores 1 and 2, which did not possess any cementum due to abrasion during the animal’s life) was removed so each transect began at the cementum-dentin junction (CDJ), and the x-values (distance in millimeters along the transect) were transformed accordingly so that each data series would begin at 0 mm. The beginning and end of each feature was determined by visual inspection of the selected image of each slab, and the distance along the transect where each feature began and ended was marked and measured using the IncMeas 1.3c plug-in (Rountrey, 2009) for ImageJ. The x- and y-values corresponding to density features were plotted in Microsoft Excel, and a second-order polynomial was fit to that graph. To remove the overall parabolic shape of a graph, the difference between the y-value of each data point and the y-value of the second-order polynomial (at the same x-value) was calculated and subsequently plotted. The resulting detrended graph shows the new y-values of the entire data set, including both the features and the background signal in between them – i.e., the relative gray values for zones of dentin that contain life history data but, unlike density features, are not characterized by dramatic fluctuations in luminance that would facilitate correlation between cores. Each annual density feature’s signature in the resulting graph was more apparent than in the graph of raw luminance values. However, even after detrending the graphs it was often still not obvious which feature in one core corresponded to a feature in an adjacent core based on visual inspection alone, because some features near the cementum and axis were still obscured. The y-axis of each detrended graph of luminance is labeled as “relative gray value” because luminance is quantified as a gray value, and because a value plotted in a detrended graph is the difference between the raw gray value and that of the second-order polynomial that was fit to the

graph of raw data. Each feature in the graphs is assigned a color, and a series of features follows the order of colors in the rainbow. Features that are matched between cores according to thin section analysis maintain their color between graphs.

While the features were not distinctive enough to match visually between cores, mathematical analysis of their patterns of relative change in luminance (their signatures) was used to obtain quantified results. The Pearson's correlation coefficient (R) was calculated to quantify the similarity of features' signatures between two adjacent cores. It was expected that a series of features in one core would have a signature most similar to that of a series of features in an adjacent core if the features were associated with the same years. It was therefore also expected that the Pearson's correlation test would yield a higher R -value when comparing accurately correlated features than when comparing features that were associated with different years. Features are referred to using a number (indicating the core in which a feature is located) followed by a lowercase letter (the alphabetical order of which indicates the relative position of a feature in the sequence of features moving away from the CDJ). This is a neutral nomenclature that does not assume any equivalencies between cores. For example, thin section analysis determined that the fourth and fifth winter-spring boundaries present in Core 3 (associated with Features 3d and 3e) are equivalent to the first and second winter-spring boundaries present in Core 4 (associated with Features 4a and 4b). Since the Pearson's correlation test requires the data sets being compared to contain an equal number of data points, the 3de data set (including all of the data points between the start of Feature 3d and the end of Feature 3e) first had to be evenly resampled because it contained more data points than the 4ab data set. The R -value could then be calculated for that hypothesis of matching. The same procedure was followed for all alternative matches of features between two cores. Table 1 shows the R -value of the hypothesized correct

match of features (indicated by “=” between feature labels) in each pair of adjacent cores compared to the R-values of all alternative matches (indicated by “≠” between feature labels).

In most cases, there are two features present in a pair of adjacent cores, with the exception of Cores 1 and 2, which only share one feature, and Cores 6 and 7 and Cores 7 and 8, which each share three features. While the only option was to calculate the R-value of just one feature present in both Cores 1 and 2, the triplets of features present in both Cores 6 and 7 (6fgh=7abc) and Cores 7 and 8 (7efg=8abc) were split into two sets of two features (6fg=7ab and 6gh=7bc, and 7ef=8ab and 7fg=8bc), and their R-values were calculated along with those of all other combinations of matches to test whether using more data points in a correlation would tend to yield a higher R-value (Table 2).

Once R was calculated for all “correct” and “incorrect” matches of features (identified on the basis of thin section analysis) between all pairs of adjacent cores, a one-tailed *t*-test assuming unequal variances was performed to test whether the group of R-values of all correct matches was significantly higher than the group of R-values of all other matches (excluding those of matches that were deemed geometrically illogical based on knowledge of pulp cavity depth and spacing of cores). This test was performed three times, all at a significance level of 0.001: once using the R-values of all three features shared between Cores 6 and 7 and Cores 7 and 8, once using the R-values of the first set of two features derived from the triplets of features, and once using the R-values of the second set of two features derived from the triplets of features.

The results of the correlation tests were evaluated based on their agreement with the results from prior thin section analysis. A photograph taken under UV light of the distal surface of each core’s Slab 3 was marked with winter-spring boundaries, and was superimposed on the image of the same core’s slice of CT data from near the distal surface of Slab 3 in ImageJ. This

showed whether or not each density feature was associated with a winter-spring boundary. When the winter-spring boundaries were included in the graphs, it could be seen whether winter-spring boundaries were located at specific landmarks within features (e.g., at the beginning of a feature), and if the relative location of a winter-spring boundary within a feature present in two cores was maintained between the two appearances of the feature.

Results

Cores 1 and 2

Between Cores 1 and 2, thin section analysis determined that Feature 1b is associated with the same year as Feature 2a ($R = 0.852$). This match of features has the highest correlation coefficient of all logical pairings (Table 1). The year boundary associated with these features is located in different positions relative to peaks in relative gray value in both graphs. It is located after the second peak in Feature 1b, and at the top of the first peak in Feature 2a (Figure 5).

Cores 2 and 3

Between Cores 2 and 3, thin section analysis determined that Features 2c and 2d are associated with the same years as Features 3a and 3b, respectively ($R = 0.293$). This match of features does not have the highest correlation coefficient of all logical pairings (Table 1). However, Features 2d and 3a were obscured by edge effects (from the reconstruction of CT data) that were too extreme to be salvaged by detrending the graphs of raw gray values. Considering the obscured features of interest and the lack of high R-values of alternative matches, the low R-value does not indicate that the 2cd=3ab hypothesis should be rejected. It is unclear if the year boundaries associated with these two features are located in similar positions relative to peaks in

relative gray value in both graphs because the signature of one feature from each pair of matched of single features (i.e., 2d in the 2d=3b match, and 3a in the 2c=3a match) is extremely obscured (Figure 6).

Cores 3 and 4

Between Cores 3 and 4, thin section analysis determined that Features 3d and 3e are associated with the same years as Features 4a and 4b, respectively ($R = 0.805$). This match of features has the highest correlation coefficient of all logical pairings (Table 1). The signature of Feature 4a was obscured by edge effects from the reconstruction of CT data, and the effect was too extreme to be salvaged by detrending the graph of raw gray values. It is unclear if the year boundary associated with the 3d and 4a density features is located in a similar position relative to peaks in relative gray value in both graphs, since Feature 4a is extremely obscured, but the year boundary associated with Features 3e and 4b is located shortly after the highest peak in both graphs (Figure 7).

Cores 4 and 5

Between Cores 4 and 5, thin section analysis determined that Features 4e and 4f are associated with the same years as Features 5a and 5b, respectively ($R = 0.333$). This match of features does not have the highest correlation coefficient of all logical pairings (Table 1). Feature 4e possesses anomalously high values of luminance seen nowhere else in the entire tusk, which calls for further study instead of the rejection of the 4ef=5ab hypothesis, since a feature with anomalous values would not result in a high R-value when compared to the values of a typical feature. Feature 5c is interrupted due to breakage that occurred during the drilling of Core 5, and

is therefore obscured in the graph of features in Core 5 and could not be used in testing alternative matches of features. Feature 4d was used in testing alternative matches of features between the two cores even though it does not contain a winter-spring boundary because it is characterized by dramatic fluctuations in attenuation like features that are associated with year boundaries, and also because its spacing between the adjacent features is similar to the spacing between typical features within the tusk. These similarities to features containing year boundaries indicate that further study is needed to assess if it could in fact be associated with a year boundary. It is unclear if the year boundary associated with Features 4e and 5a is located in a similar position relative to peaks in relative gray value in both graphs because Feature 4e has anomalous values, but the year boundary associated with Features 4f and 5b is located after the first peak in Feature 4f and before the first peak in Feature 5b (Figure 8).

Cores 5 and 6

Between Cores 5 and 6, thin section analysis determined that Features 5e and 5f are associated with the same years as Features 6b and 6c, respectively ($R = 0.672$). This match of features has the highest correlation coefficient of all logical pairings (Table 1). Only a fraction of Feature 6a is present in the core and although its winter-spring boundary is contained in the core, an incomplete feature is not suitable for correlation with a complete feature in an adjacent core, so it was excluded from this analysis. The year boundary associated with Features 5e and 6b is located at the second peak in the graph of relative gray value in Feature 5e and after the second peak in Feature 6b, and the year boundary associated with Features 5f and 6c is located at the second peak in Feature 5f and after the second peak in Feature 6c (Figure 9).

Cores 6 and 7

Between Cores 6 and 7, thin section analysis determined that Features 6f, 6g, and 6h are associated with the same years as Features 7a, 7b, and 7c, respectively ($R = 0.673$). This match of features has the highest correlation coefficient of all logical pairings (Table 1). Since three features are shared between these two cores, the triplets of features were split into two sets of two features (i.e., 6fgh was split into 6fg and 6gh, and 7abc was split into 7ab and 7bc) and the correlation coefficients of the pairs of features between cores were tested in addition to the triplets of features to determine if the correlation coefficient between the triplets of features was artificially high due to correlating longer data sets (Table 2). The R-value of the 6fg and 7ab data sets is 0.669, and is the highest correlation coefficient of all logical matches. The R-value of the 6gh and 7bc data sets is 0.682, and is the highest correlation coefficient of all logical matches. These results indicate that the correlation coefficient of the data sets of triplets of features, 6fgh and 7abc, is not artificially high. It is unclear if the year boundary associated with Features 6f and 7a is located in the same position relative to peaks in relative gray value in both graphs since Feature 7a was obscured even after detrending the graph of raw gray values, but the year boundary associated with Features 6g and 7b is located after the first peak in Feature 6g and at the top of the first peak in Feature 7b, and the year boundary associated with Features 6h and 7c is located after the highest peak in Feature 6h and at the top of the highest peak in Feature 7c (Figure 10).

Cores 7 and 8

Between Cores 7 and 8, thin section analysis determined that Features 7e, 7f, and 7g are associated with the same years as Features 8a, 8b, and 8c, respectively ($R = 0.712$). This match

of features has the highest correlation coefficient of all logical pairings (Table 1). Since three features were shared between these two cores, the triplets of features were split into two sets of two features (i.e., 7efg was split into 7ef and 7fg, and 8abc was split into 8ab and 8bc) and the correlation coefficients of the pairs of features between cores (7ef compared to 8ab, and 7fg compared to 8bc) were tested in addition to the triplets of features to determine if the correlation coefficient between the triplets of features was artificially high due to correlating longer data sets (Table 2). The R-value of the 7ef and 8ab data sets is 0.607, and is the highest correlation coefficient of all logical matches. The R-value of the 7fg and 8bc data sets is 0.641, and is the highest correlation coefficient of all logical matches. These results indicate that the correlation coefficient of the data sets of triplets of features, 7efg and 8abc, is not artificially high. Features 7f and 7g have notably similar signatures compared to those of Features 8b and 8c, respectively. It is unclear if the year boundary associated with Features 7e and 8a is located in the same position relative to peaks in relative gray value in both graphs since Feature 7e is obscured even after detrending the graph of raw gray values, but the year boundary associated with Features 7f and 8b is located after the last peak in Feature 7f and at the top of the penultimate peak in Feature 8b, and the year boundary associated with Features 7g and 8c is located at the top of the last peak in Feature 7g and after the last peak in Feature 8c (Figure 11).

Summary of Results

In five out of the seven pairs of adjacent cores, the correct correlation of annual increments of dentin according to thin section analysis possesses the highest correlation coefficient of the density features associated with those annual increments compared to other logical pairings of features. The two pairs of adjacent cores in which the correct match of annual

increments according to thin section analysis does not possess the highest correlation coefficient of density features, Cores 2 and 3 and Cores 4 and 5, have special circumstances that affected the correlation coefficients (see above and Discussion), and therefore the hypotheses formed from the results of thin section analyses are not rejected. Even considering the low correlation coefficients of the provisionally correct match of features in Cores 2 and 3 and Cores 4 and 5, the set of correlation coefficients of all correct matches of features in all pairs of cores is statistically significantly higher than the set of correlation coefficients of all other logical matches of features. A one-tailed *t*-test, assuming unequal variances, was performed to quantify the difference between the two sets of values. To ensure that using different numbers of features between Cores 6 and 7 and Cores 7 and 8 did not significantly impact the results, the *t*-test was performed three times, all with a significance level of 0.001. In the first *t*-test, using the correlation coefficient of all three features present between Cores 6 and 7 (6fgh=7abc) and Cores 7 and 8 (7efg=8abc) against alternative matches of three features, the resulting p-value is 0.00018. In the next *t*-test, using the correlation coefficient of the first pair in each triplet of features present between Cores 6 and 7 (6fg=7ab) and Cores 7 and 8 (7ef=8ab) against alternative matches of two features, the resulting p-value is 0.00011. In the final *t*-test, using the correlation coefficient of the second pair in each triplet of features present between Cores 6 and 7 (6gh=7bc) and Cores 7 and 8 (7fg=8bc) against alternative matches of two features, the resulting p-value is 0.00016. All of the *t*-tests show that the set of correlation coefficients of correct matches of features is statistically significantly higher than the set of correlation coefficients of all other matches that were not geometrically illogical, regardless of how many features are used in matches between Cores 6 and 7 and Cores 7 and 8.

The location of a winter-spring boundary associated with a density feature present in two adjacent cores was expected to be in the same position relative to landmarks in the graphs of luminance. While the winter-spring boundary is always within each density feature, with the exception of Feature 4d in which thin section analysis did not identify a year boundary, it is often not in the same relative position within a feature in one core as it is within the equivalent feature in an adjacent core. Also, winter-spring boundaries are not associated with any particular location within density features (i.e., they are not consistently present at the beginning, middle, or end of a feature, nor are they consistently present at the relative maximum or minimum relative gray value within a feature). This apparent lack of a pattern in the location of winter-spring boundaries within density features suggests that further study is needed to fully understand the processes of dentin apposition and mineralization and how they may differ along the length of the pulp cavity.

Discussion

In five of the seven pairs of adjacent cores analyzed in this study, the correct match of features between cores according to thin section analysis has the highest correlation coefficient of all logical matches. The logical status of a match of features between adjacent cores is based on knowledge of tusk pulp cavity depth and geometry, and the distance between cores taken along the length of the tusk. The tusk pulp cavity of the Yukagir mammoth, and therefore each conical increment of dentin, is approximately 45 cm long in much of the tusk, and most of the cores were taken 30 cm apart. Based on this knowledge, the two features nearest the CDJ in one core could not possibly be the correct match for the two features nearest the CDJ in an adjacent core. For example, the 3ab≠4ab match has a high R-value (0.608), but for 3ab to be equivalent to

4ab, considering that Cores 3 and 4 were taken 30 cm apart, the pulp cavity would have to be nearly infinitely deep. An exception to this logic is when a core does not contain any cementum due to abrasion, such as in Cores 1 and 2, since years of dentin may have been abraded away as well. In such cases, a match of features is less likely to be deemed illogical. Any alternative matches of features that are deemed illogical (cells with dark gray fill in Tables 1 and 2) can be ignored, even if their correlation coefficients are higher than that of the correct match of features. Some alternative matches (cells with light gray fill in Tables 1 and 2) are also likely illogical, but to be conservative, their correlation coefficients are still considered. High correlation coefficients in illogical alternative matches, like $3ab \neq 4ab$, are likely the result of the general downward-sloping trend of features close to the CDJ due to edge effects from the reconstruction of CT data that could not be eliminated by detrending the graphs. Other matches of features near the middle of slabs (i.e., not affected by edge effects), like the illogical match of $5ef \neq 6fg$ in which $R = 0.746$, can be ignored based on knowledge of pulp cavity depth. Since illogical matches sometimes have correlation coefficients higher than the correct match of features, this method of analysis would not be useful in a study where the distance between cores is unknown, because this would prevent identification of illogical matches.

In two of the seven pairs of adjacent cores analyzed in this study (between Cores 2 and 3 and between Cores 4 and 5), the correct match of features between cores according to thin section analysis does not have the highest correlation coefficient of all logical matches. The correct match according to thin section analysis of features between Cores 2 and 3 is $2cd = 3ab$, but the R-value of that match is only 0.293. The correlation coefficient of $2ab \neq 3ab$ is 0.552, which is higher than the correct match. This is likely an illogical correlation, but there is no cementum present in Core 2 due to abrasion, so the $2ab \neq 3ab$ match is not deemed illogical since

dentin may have been lost to abrasion as well. The correlation coefficient of $2bc \neq 3ab$ is 0.487, which is also higher than the correct match. This is a geometrically plausible match of features, which could cast some doubt on the correct match. While the R-value of the correct match is low and does not confirm the correlation made by thin section analysis, the $2cd = 3ab$ hypothesis is not rejected because the features of interest were extremely obscured by edge effects from reconstruction of CT data. Even after the graphs of Cores 2 and 3 were detrended, Feature 2d was still obscured by the artificially positive trend of the portion of the graph where it is located, and Feature 3a was obscured in the same way, except by the negative trend (Figure 6). The 2c-3a half of the match could not result in a high correlation because the luminance profile of Feature 3a was not accurate, and the 2d-3b half of the match could not result in a high correlation because the luminance profile of Feature 2d was not accurate. Therefore, the correct match of features according to thin section analysis is not refuted by these results.

The correct match of features according to thin section analysis between Cores 4 and 5 also does not have the highest correlation coefficient of all logical alternative matches. The correct match, $4ef = 5ab$, has a correlation coefficient of only 0.333. The correlation coefficient of $4cd \neq 5ab$, a geometrically plausible match, is 0.664, which could cast some doubt on the result from thin section analysis. While the low correlation coefficient does not confirm the correct match according to thin section analysis, the $4ef = 5ab$ hypothesis is not rejected because two features in Core 4 call for further analysis of the core. Feature 4d appears to be a typical feature considering its fluctuations in radiodensity and its spacing between adjacent features, but when the winter-spring boundaries were plotted along the transect drawn across Core 4, no year boundary was found to be associated with Feature 4d. A winter-spring boundary was found within every other feature in this study. Another issue is the anomalous luminance values of

Feature 4e. Its values are dramatically higher than those of any other feature in any core, and dramatically higher than its corresponding feature in Core 5 (Figure 8). There is no apparent crack in the dentin at its location in the slab (although there is a markedly bold band near its location) and it does not appear to be an artifact from CT reconstruction. The questions concerning Features 4d and 4e call for further analysis before the 4ef=5ab hypothesis can be confirmed or rejected.

While this method of correlation of years between cores via microCT generally yielded positive results, it did come with challenges. Cores 9, 10, and 11 could not be used in this study because they are broken into pieces due to desiccation. While they yielded data in prior thin section analysis, the CT scans showed that they delaminated along layers of dentin, and each feature was obscured. Thus, this method is likely not useful for specimens that are not reasonably well-preserved or that have significant fracturing. In intact cores, the main difficulty was correcting for the overall parabolic shape of the graphs that was caused by edge effects from the reconstruction of CT data. The 3D reconstruction of each slab is significantly brighter at the outer surface of the slab containing the cementum and at the cut surface near the axis (Figure 4a) and therefore resulted in parabolic graphs of luminance along the transect that do not accurately depict the radiodensity of the dentin (Figure 4b). Detrending the graphs did make the features more apparent, but in many cases, it was impossible to completely elucidate the features close to the cementum and axis. This was a significant difficulty because the features near the cementum and axis are the features of particular interest in this study, as they are the features shared between adjacent cores. In longer cores that contain more annual increments of dentin, like Cores 6, 7, and 8, more features could be matched between them, so it was less problematic that the features close to the edges of each slab were still partially obscured. In cores that contain fewer

annual increments, like Cores 1, 2, and 3, there were fewer features shared by adjacent cores, which made them more difficult to correlate as sometimes the only features available for matching were obscured (e.g., between Cores 2 and 3 in which the correct match had a low correlation coefficient).

In addition to issues with the CT data, the natural thinning of annual increments of dentin as they approach the cementum compressed the density features associated with them. Although the data sets of a feature present nearer to the axis in one core and nearer to the cementum in the adjacent, more proximally-located core were resampled, it is still often difficult to visualize the similarities in the signature of the feature as it appears in graphs of both cores. Another possible explanation for the dissimilarity of the signature of a feature matched between cores is that the density within layers of dentin may vary slightly along its full length in the tusk due to dentin formation not being as uniform along the surface of the pulp cavity as expected. This may also account for the winter-spring boundary being positioned in different locations relative to landmark peaks in luminance in one feature present in two cores. However, the locations of winter-spring boundaries were determined by analysis of the heels of the cores and were then translated onto photographs of the distal surface of Slab 3 of each core, and were translated again onto images of slices of CT data taken from near the distal surface of Slab 3, so it is conceivable that there could have been some error in the placement of the exact locations of the winter-spring boundaries along the transects. The inconsistencies in the locations of winter-spring boundaries call for further study of dentin apposition and mineralization along the length of the pulp cavity.

To increase the usefulness of this method in future studies, sampling a tusk at close intervals to increase the amount of overlap of features between cores is arguably the most important factor. This study is a severe test of this method because adjacent cores do not have

very much overlap of annual increments. The tusk pulp cavity of this individual is around 45 cm deep, and most of the cores were taken 30 cm apart. In other specimens, cores are often taken closer together. In some female specimens, where the pulp cavities may be only approximately 20 cm deep, the cores are taken at 10 cm intervals, so there is more overlap of annual dentin increments, which would enable more confident correlation of increments between cores. In this study, the presence of artifacts from the CT reconstruction due to beam hardening resulted in artificially high luminance near the cementum and near the tusk axis of each slab, which obscured the density features in those portions of the slabs. Since the cores in this study were spaced far apart relative to the length of the increments in the tusk, the density features that are contained in two adjacent cores are located near the cementum and near the axis (i.e., in the areas of the slabs that were obscured by CT artifacts). Thus, while correlation of annual increments by microCT analysis was sometimes difficult in this study, it is expected to be easier in specimens that are sampled at closer intervals. Furthermore, analysis of microCT data is less time-consuming than analysis of thin sections, and therefore microCT may be a preferable method of analysis for correlating years between cores.

Conclusions

The Yukagir mammoth's tusks are well-preserved, but three of the eleven cores were unsuitable for analysis of density features within the dentin since they were broken due to desiccation and the density features were obscured. The density features in the eight intact cores were readily apparent in microCT scans. In five out of seven pairs of adjacent cores, the correct match of features according to thin section analysis has the highest correlation coefficient among all logical matches. In two pairs of adjacent cores, the correct match of features according to thin

section analysis does not have the highest correlation coefficient. The correct match of features between Cores 2 and 3 has a low correlation coefficient due to edge effects (from the reconstruction of CT data) obscuring the features of interest even after detrending the graphs. That issue could be solved by sampling a tusk at relatively closer intervals. The correct match of features between Cores 4 and 5 has a low correlation coefficient due to the anomalous nature of Features 4d and 4e, which call for further study. This method successfully shows that the correct match of increments of dentin between adjacent cores established by thin section analysis has the most similar pattern of density of any alternative matches that are geometrically logical. The factor that most significantly inhibited correlation was the obscurity of features dominated by edge effects, which would be less problematic if the cores had been taken closer together to allow features shared by two cores to be present closer to the middle of slabs where features are not obscured. It is worthwhile to study the density of tusk cores via microCT of any specimen that is reasonably well-preserved since microCT yields unique data that cannot be seen in thin section. This study is a rigorous test of this novel method of correlation, and its results indicate that future studies on tusks that are only available for study via discrete samples would also be successful.

Acknowledgments

I would like to thank my advisor, Daniel Fisher, for his support and guidance throughout this study, and for reviewing my thesis along with William Sanders, whose support I am also grateful for. Additional thanks to Scott Beld for his photography of specimens and analysis of thin sections, and to Martin Jones for his expertise in microCT and for use of the CT scanner at Ford Motor Company. Finally, I would like to thank my colleagues and friends Ethan Shirley,

Fabian Hardy, and Martin Arlt for their valuable comments on my thesis and their unwavering support of my scientific endeavors.

References

- Cherney, M.D., Fisher, D.C., Rountrey, A.N., 2017. Tusk pairs in the Ziegler Reservoir mastodon (*Mammot americanum*) assemblage: implications for site taphonomy and stratigraphy. *Quaternary International* 443, 168–179. doi:10.1016/j.quaint.2016.10.041
- El Adli, J.J., Cherney, M.D., Fisher, D.C., Harris, J.M., Farrell, A.B., Cox, S.M., 2015. Last years of life and season of death of a Columbian mammoth from Rancho La Brea. *Science Series* 42, 65–80.
- El Adli, J.J., Fisher, D.C., Vartanyan, S.L., Tikhonov, A.N., 2017a. Final years of life and seasons of death of woolly mammoths from Wrangel Island and mainland Chukotka, Russian Federation. *Quaternary International* 445, 135–145. doi:10.1016/j.quaint.2016.07.017
- El Adli, J.J., Fisher, D.C., Cherney, M.D., Labarca, R., Lacomat, F., 2017b. First analysis of life history and season of death of a South American gomphothere. *Quaternary International* 443, 180–188. doi:10.1016/j.quaint.2017.03.016
- Fisher, D., Rountrey, A., Beld, S., Fox, D., Gohman, S., Tikhonov, A., Mol, D., Buigues, B., Boeskorov, G., Lazarev, P., 2010. Life history of the Yukagir mammoth. In: *Proceedings of the IV International Mammoth Conference*. pp. 54–63.
- Fisher, D.C., 1984. Taphonomic analysis of late Pleistocene mastodon occurrences: evidence of butchery by North American Paleo-Indians. *Paleobiology* 10, 338–357. doi:10.1017/s0094837300008319
- Fisher, D.C., 1987. Mastodont procurement by Paleoindians of the Great Lakes Region: hunting or scavenging? In: Nitecki, M.H., Nitecki, D.V. (Eds.), *The Evolution of Human Hunting*. Plenum, New York, pp. 309–421.
- Fisher, D.C., 1996. Extinction of proboscideans in North America. In: Shoshani, J., Tassy, P. (Eds.), *The Proboscidea: Evolution and Palaeoecology of Elephants and Their Relatives*. Oxford University Press, Oxford, pp. 296–315.
- Fisher, D.C., 2001. Season of death, growth rates, and life history of North American mammoths. In: West, D. (Ed.), *Proceedings of the International Conference On Mammoth Site Studies*. University of Kansas, Lawrence, pp. 121–135.
- Fisher, D.C., 2007. Life history analysis of the Yukagir mammoth. In: Boeskorov, G.G., Tikhonov, A.N., Suzuki, N. (Eds.), *The Yukagir Mammoth*. Saint Petersburg, pp. 142–156.
- Fisher, D.C., 2009. Paleobiology and extinction of proboscideans in the Great Lakes region of North America. In: Haynes, G. (Ed.), *American Megafaunal Extinctions at the End of the Pleistocene*. Springer, New York, pp. 55–75.

- Fisher, D.C., 2018. Paleobiology of Pleistocene proboscideans. *Annual Review of Earth and Planetary Sciences* 46, 229–260. doi:10.1146/annurev-earth-060115-012437
- Fisher, D.C., Fox, D.L., 2006. Five years in the life of an Aucilla River mastodon. In: Webb, S.D. (Ed.), *First Floridians and Last Mastodons: The Page-Ladson Site in the Aucilla River*. Springer, pp. 343–377. doi:10.1007/978-1-4020-4694-0_12
- Fisher, D.C., Fox, D.L., 2007. Season of death of the Dent mammoths. In: Brunswig, Pitblado (Eds.), *Frontiers in Colorado Paleoindian Archaeology: From the Dent Site to the Rocky Mountains*. University of Colorado Press, Boulder, pp. 123–154.
- Fisher, D.C., Cherney, M.D., Newton, C., Rountrey, A.N., Calamari, Z.T., Stucky, R.K., Lucking, C., Petrie, L., 2014. Taxonomic overview and tusk growth analyses of Ziegler Reservoir proboscideans. *Quaternary Research (United States)* 82, 518–532. doi:10.1016/j.yqres.2014.07.010
- Fox, D.L., Fisher, D.C., 1994. Tusk growth rate in *Loxodonta africana* as recorded by incremental laminae in tusk dentin. *Journal of Vertebrate Paleontology* 14, 26A.
- Koch, P.L., Fisher, D.C., Dettman, D., 1989. Oxygen isotope variation in the tusks of extinct proboscideans: a measure of season of death and seasonality. *Geology* 17, 515–519. doi:10.1130/0091-7613(1989)017<0515:OIVITT>2.3.CO;2
- Racicot, R., 2016. Fossil secrets revealed: X-ray CT scanning and applications in paleontology. *The Paleontological Society Papers* 22, 21–38. doi:10.1017/scs.2017.6
- Rasband, W.S., 1997. ImageJ. United States National Institutes of Health, Bethesda, Maryland. <http://imagej.nih.gov/ij/>.
- Rountrey, A.N., 2009. Life Histories of Juvenile Woolly Mammoths from Siberia: Stable Isotope and Elemental Analyses of Tooth Dentin. Ph.D. dissertation. University of Michigan. xiii+331.
- Smith, K.M., Fisher, D.C., 2011. Sexual dimorphism of structures showing indeterminate growth: tusks of American mastodons (*Mammuth americanum*). *Paleobiology* 37, 175–194.
- Smith, K.M., Fisher, D.C., 2013. Sexual dimorphism and inter-generic variation in proboscidean tusks: multivariate assessment of American mastodons (*Mammuth americanum*) and extant African elephants. *Journal of Mammalian Evolution* 20, 337–355. doi:10.1007/s10914-013-9225-6

Figures and Tables

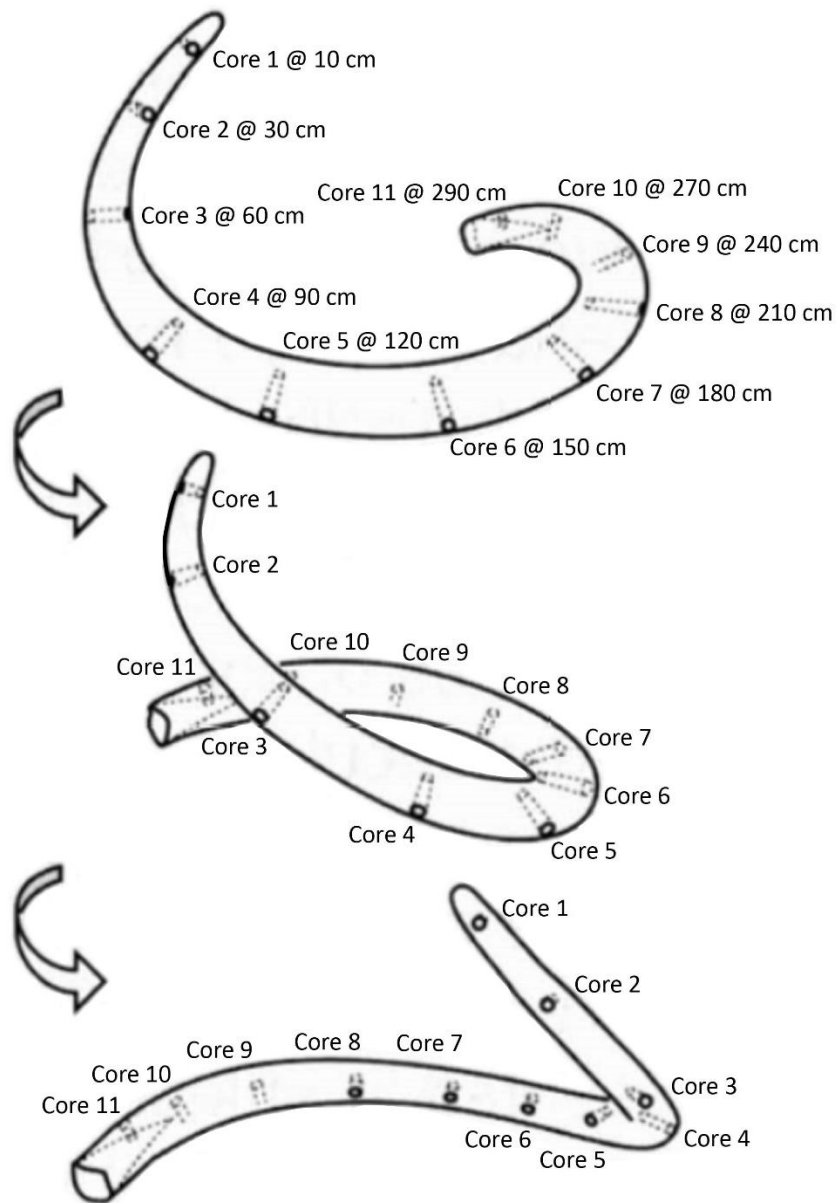


Figure 1. Three views of locations of the eleven cores taken from the right tusk of the Yukagir mammoth. Tusk is illustrated as if placed on a turntable at ground level and viewed by a standing observer as the table turns. Bottom view roughly approximates a dorsal aspect, but other views are non-standard. Top view is labeled with both the core number and the distance from tusk tip at which the core was taken. Middle and bottom views are only labeled with the core number. Modified from Figure 1a in Fisher et al., 2010.

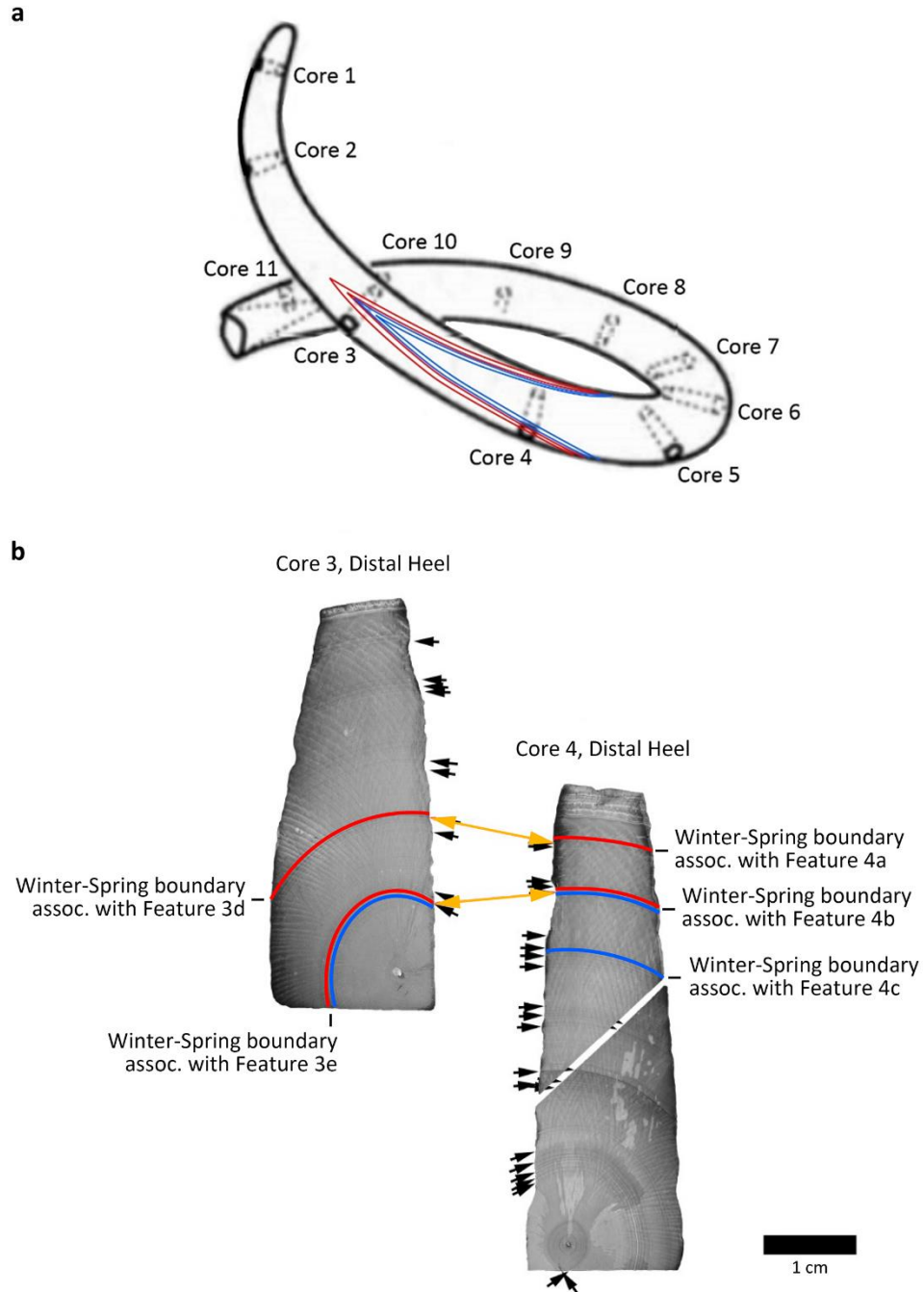


Figure 2. (a) Cross sectional (2-dimensional) view of two annual increments of dentin (red and blue areas) present in Cores 3 and 4 (shown in the context of a perspective view of the entire tusk). Modified from Figure 1a in Fisher et al., 2010. (b) Same two annual increments as seen in thin sections made from Distal Heels of Cores 3 and 4 under UV light. Distal Heel of Core 3 has been flipped horizontally to facilitate visual correlation of annual increments. Black arrows point to distinctive sub-annual increments. Gold arrows connect distinctive sub-annual increments that were matched between Cores 3 and 4.

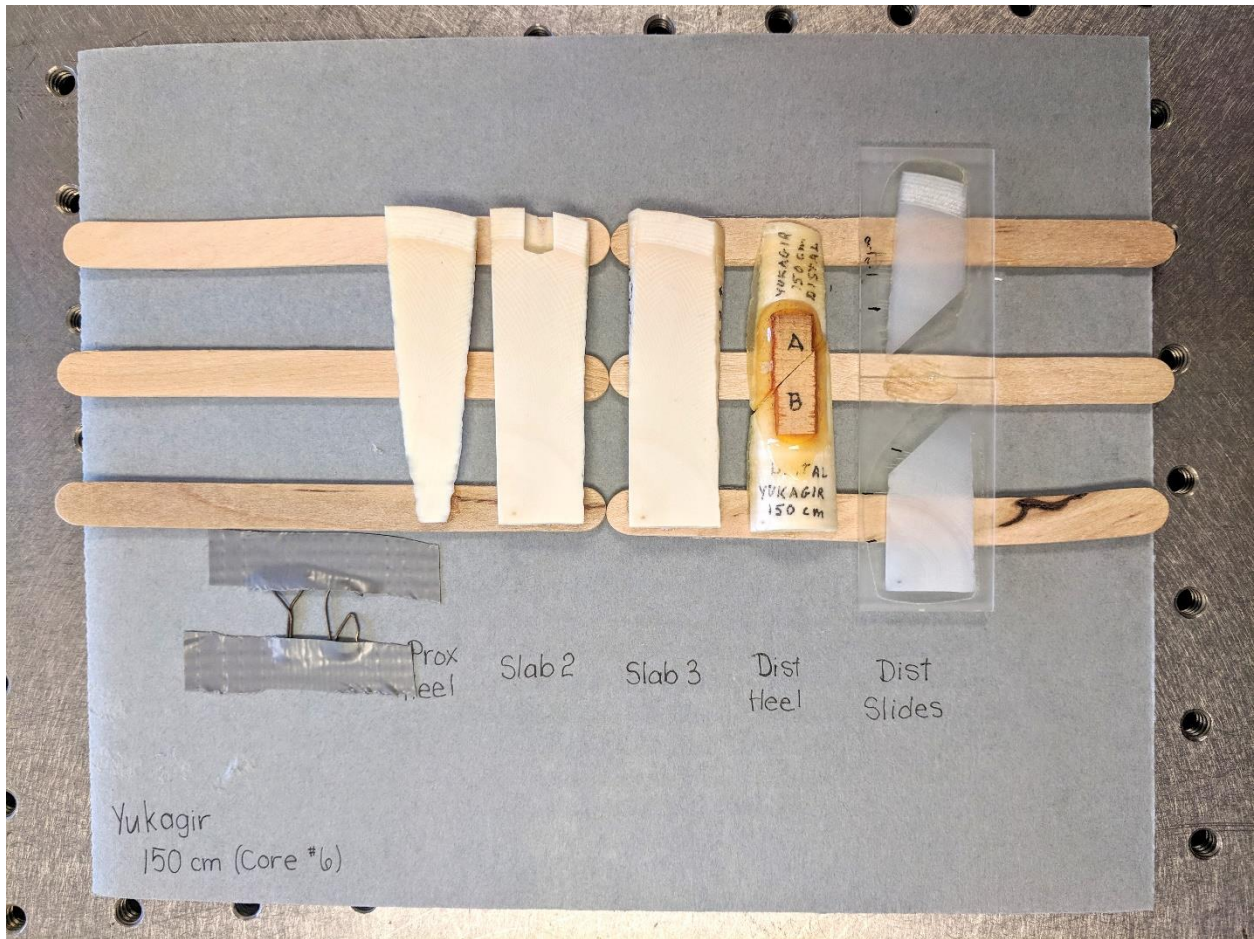


Figure 3. Setup of the four slabs (Slab 1/Proximal Heel, Slab 2, Slab 3, and Slab 4/Distal Heel) of Core 6 prior to scanning. Slabs laid out from left to right, maintaining orientation of cut surfaces. Cardboard sheet labeled “Y6” in copper wire to record specimen name and core number.

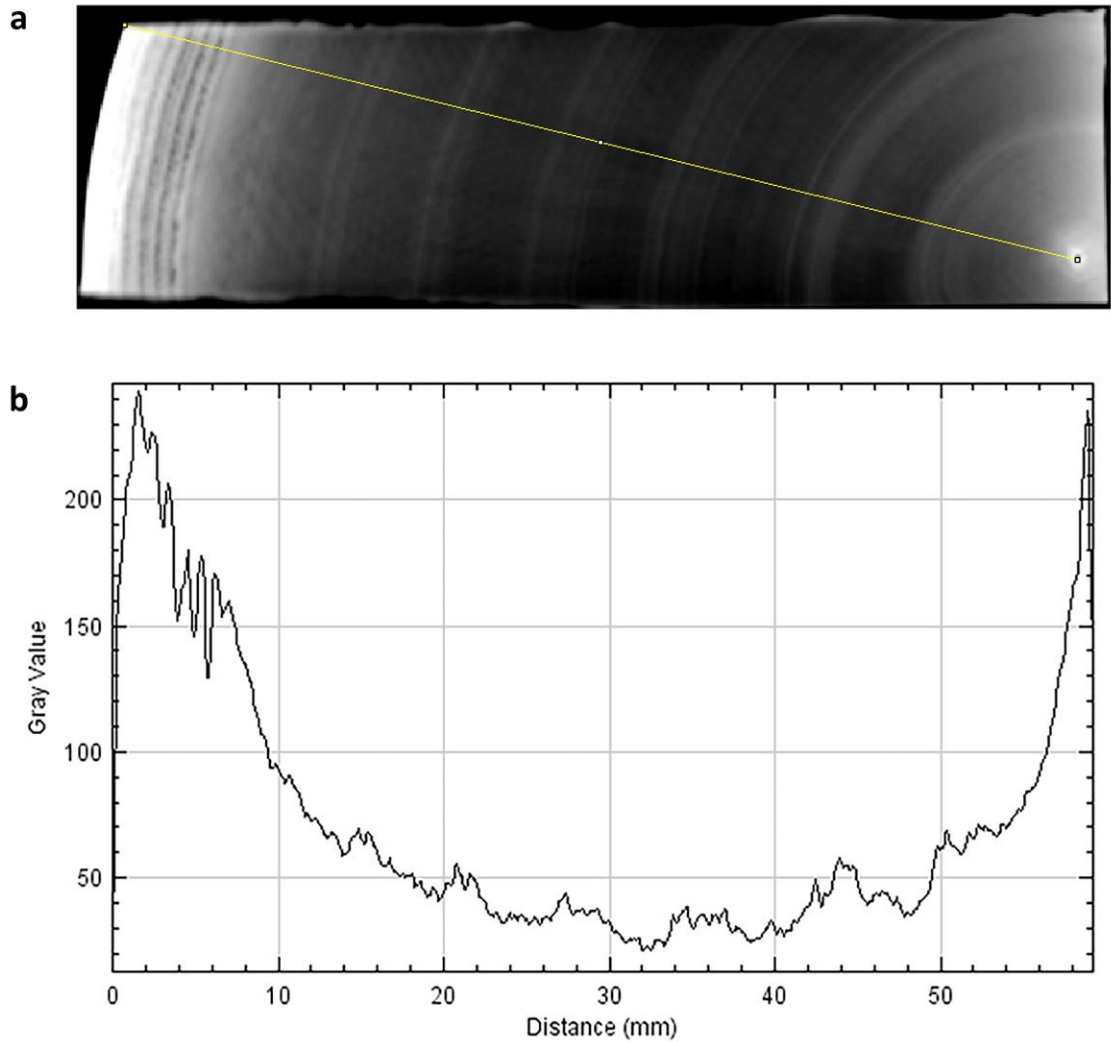


Figure 4. (a) Slice of CT data from near distal surface of Slab 3 of Core 6, perpendicular to annual increments of dentin. Transect drawn perpendicular to density features. Areas of higher radiodensity expressed as pixels with greater luminance. (b) Graph of gray value along transect drawn in panel a.

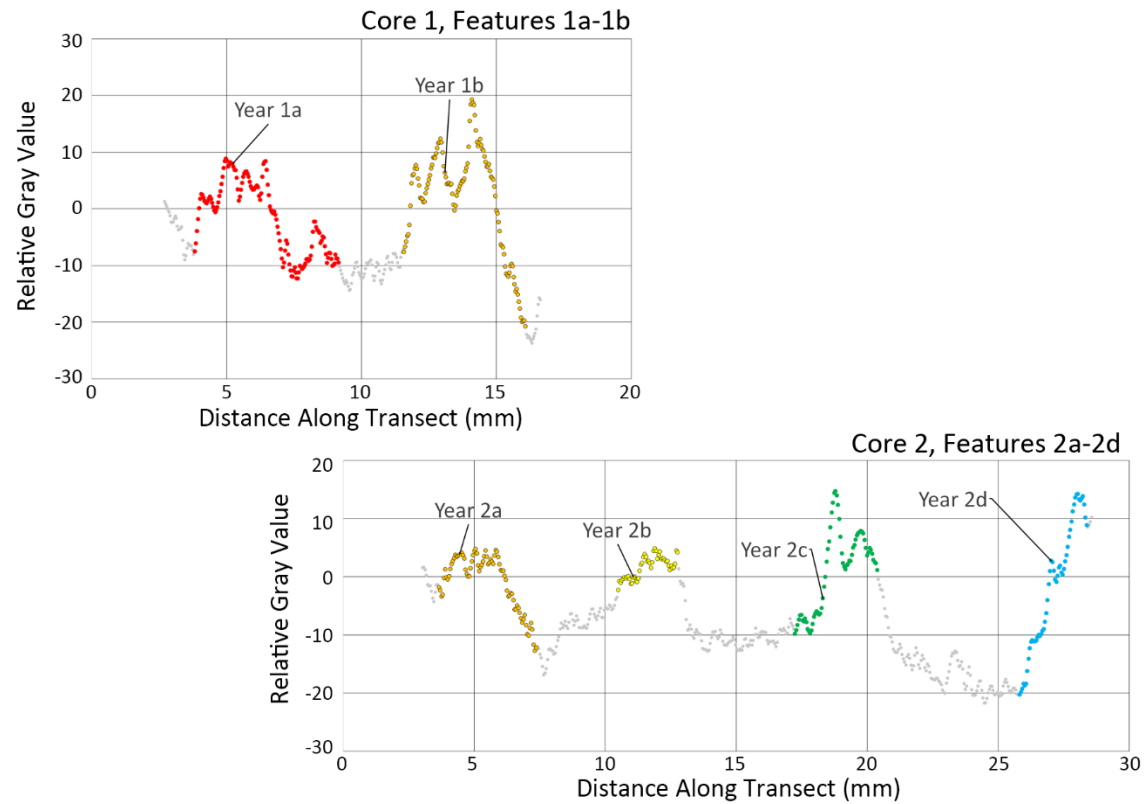


Figure 5. Detrended graphs of gray value along transects across Cores 1 and 2. Data corresponding to density features plotted in color. Year boundary associated with each feature labeled with the corresponding density feature identifier. Graphs staggered and color-coded to facilitate visual correlation of Features 1b and 2a.

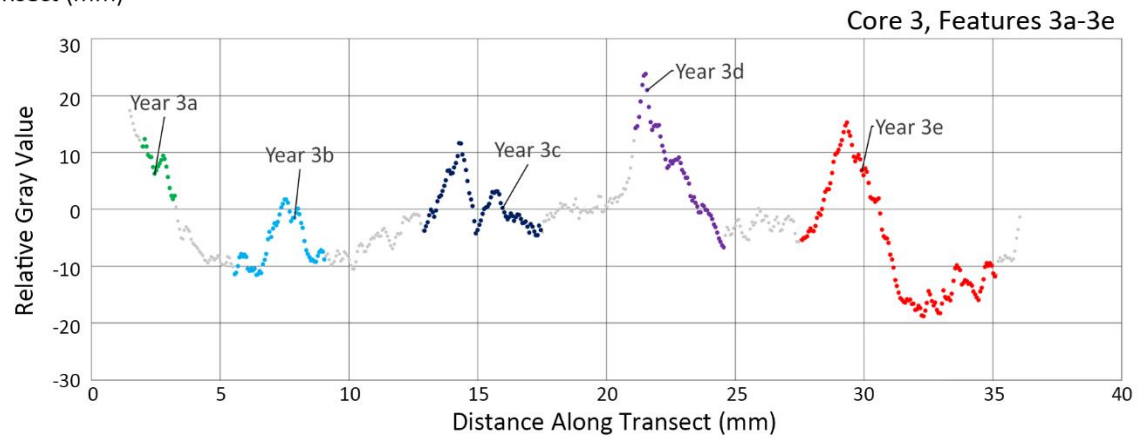
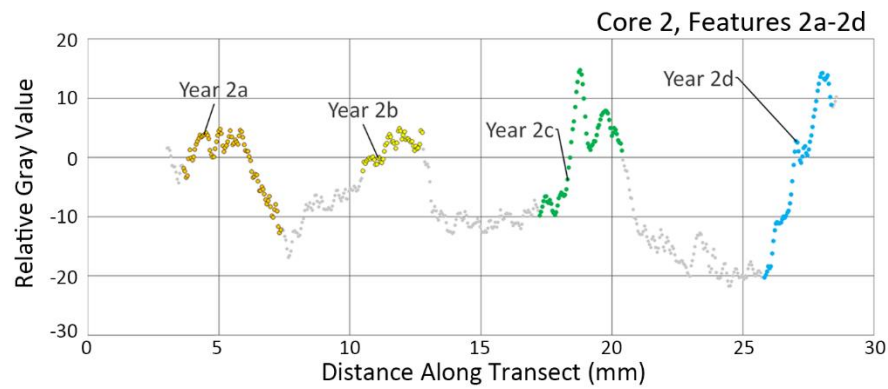


Figure 6. Detrended graphs of gray value along transects across Cores 2 and 3. Data corresponding to density features plotted in color. Year boundary associated with each feature labeled with the corresponding density feature identifier. Graphs staggered and color-coded to facilitate visual correlation of Features 2cd and 3ab.

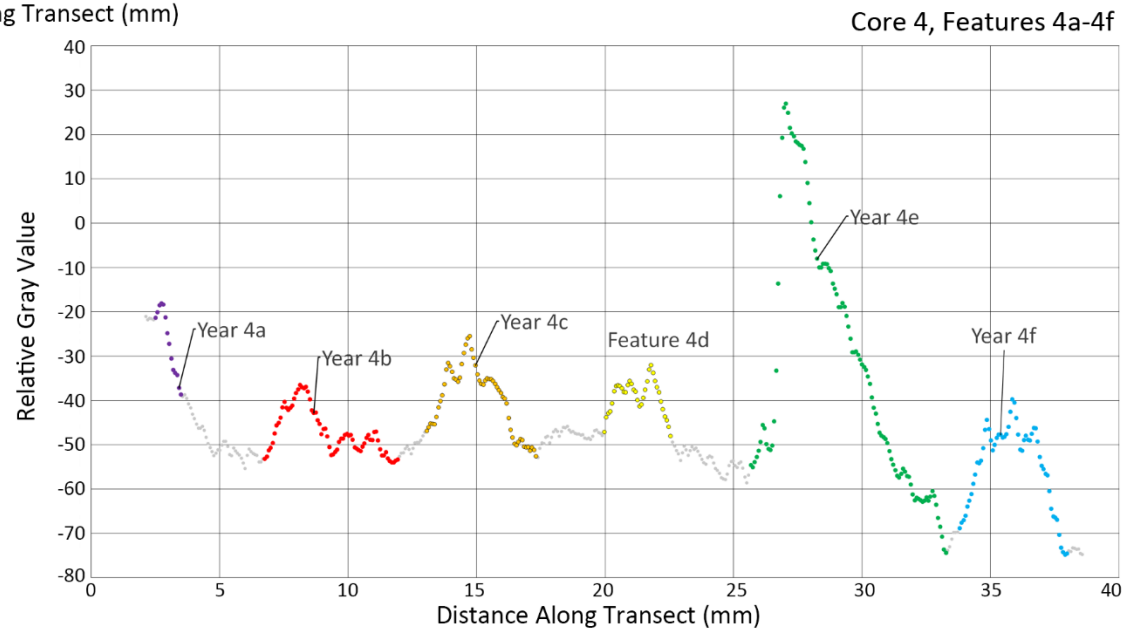
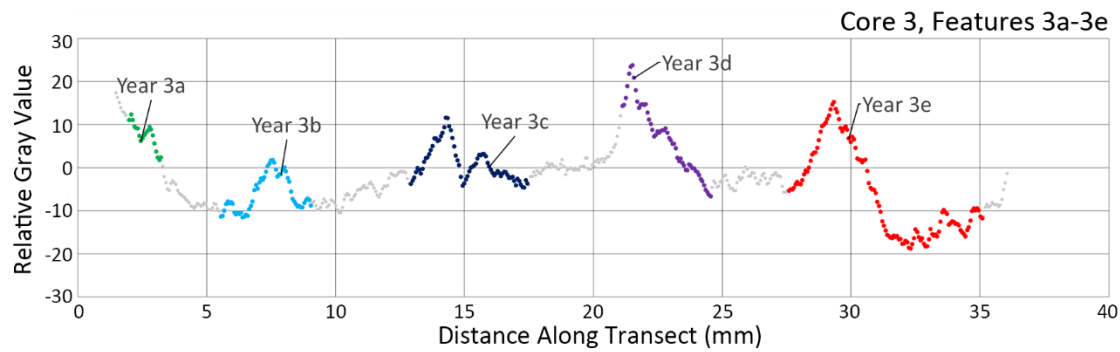


Figure 7. Detrended graphs of gray value along transects across Cores 3 and 4. Data corresponding to density features plotted in color. Year boundary associated with each feature labeled with the corresponding density feature identifier. No year boundary identified within Feature 4d. Graphs staggered and color-coded to facilitate visual correlation of Features 3de and 4ab.

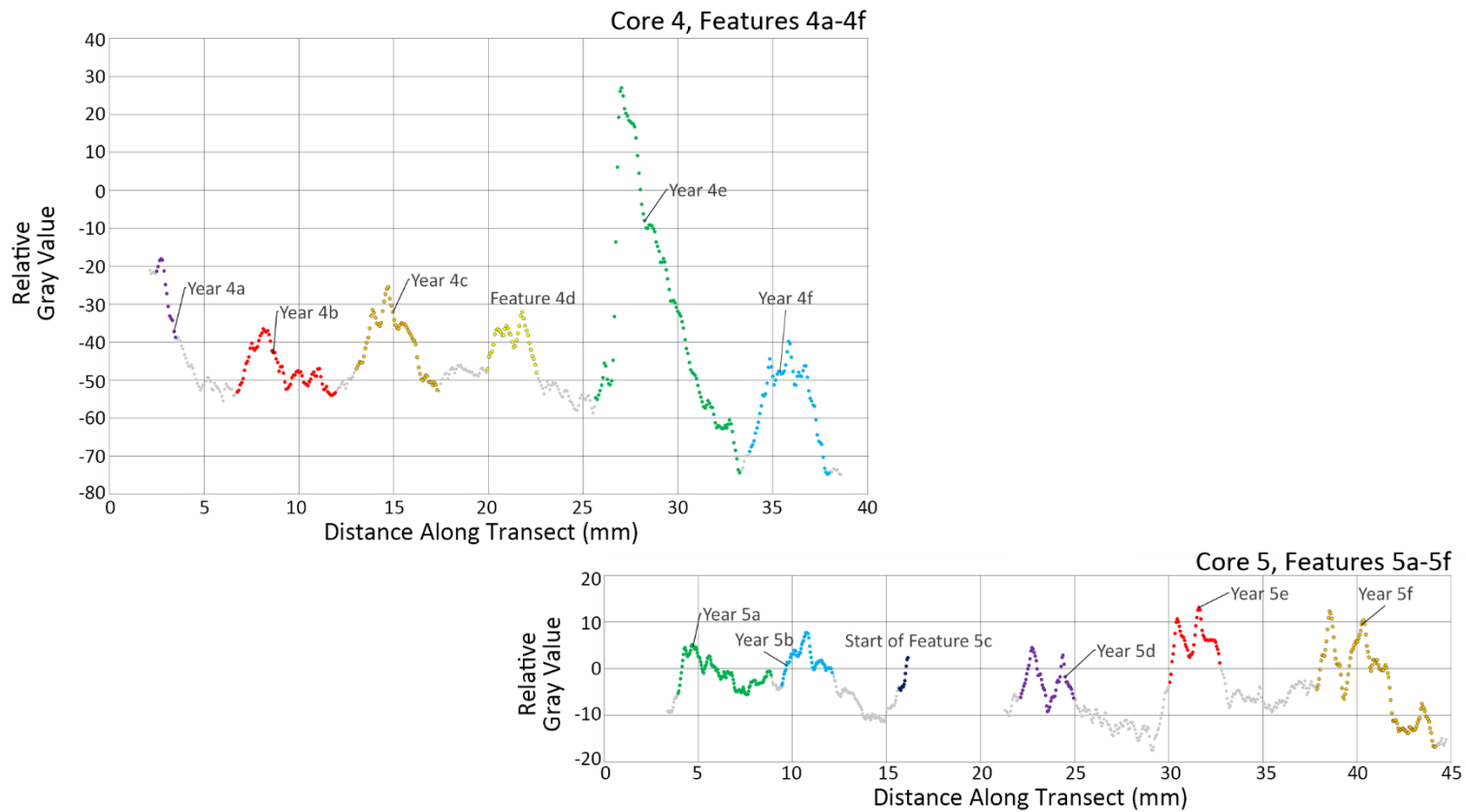


Figure 8. Detrended graphs of gray value along transects across Cores 4 and 5. Data corresponding to density features plotted in color. Year boundary associated with each feature labeled with the corresponding density feature identifier. No year boundary identified within Feature 4d. Feature 5c interrupted due to breakage of core during sampling. Graphs staggered and color-coded to facilitate visual correlation of Features 4ef and 5ab.

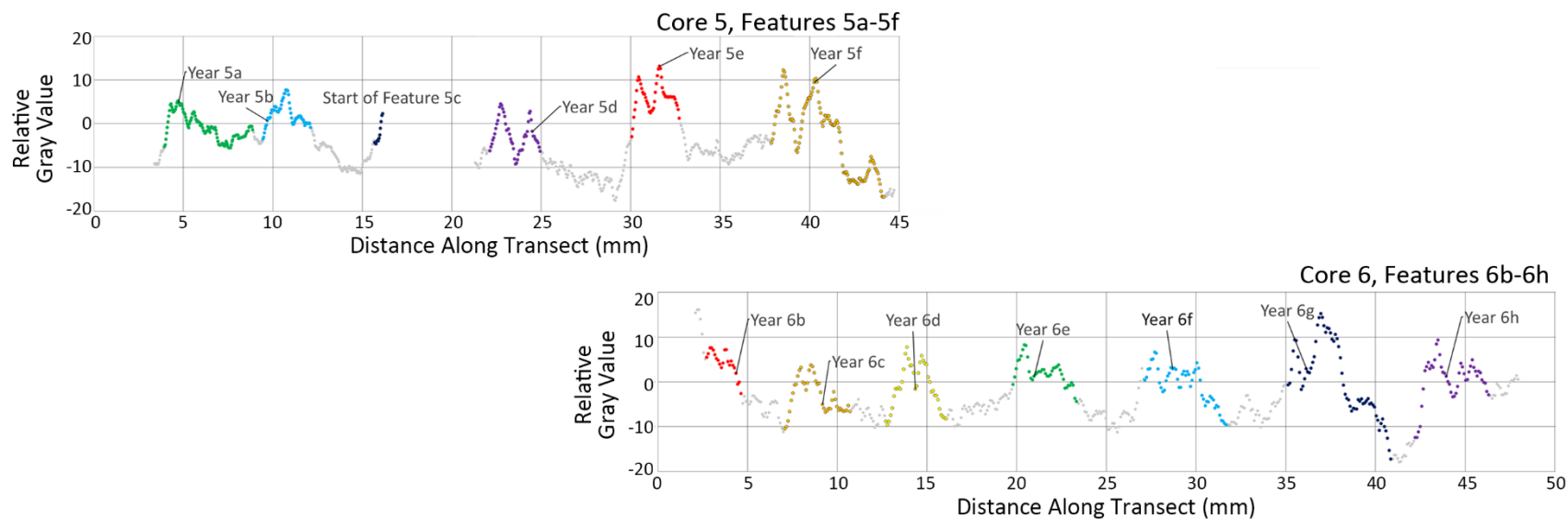


Figure 9. Detrended graphs of gray value along transects across Cores 5 and 6. Data corresponding to density features plotted in color. Year boundary associated with each feature labeled with the corresponding density feature identifier. Feature 5c interrupted due to breakage of core during sampling. Feature 6a omitted due to incomplete appearance in core. Graphs staggered and color-coded to facilitate visual correlation of Features 5ef and 6bc.

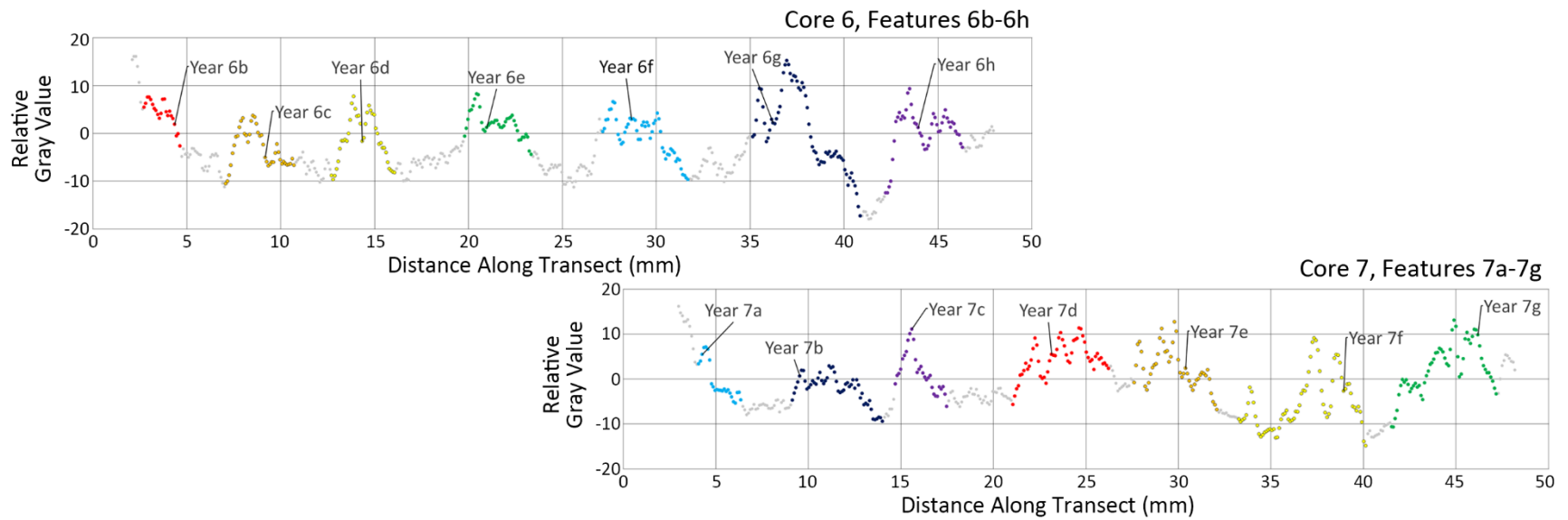


Figure 10. Detrended graphs of gray value along transects across Cores 6 and 7. Data corresponding to density features plotted in color. Year boundary associated with each feature labeled with the corresponding density feature identifier. Feature 6a omitted due to incomplete appearance in core. Graphs staggered and color-coded to facilitate visual correlation of Features 6fgh and 7abc.

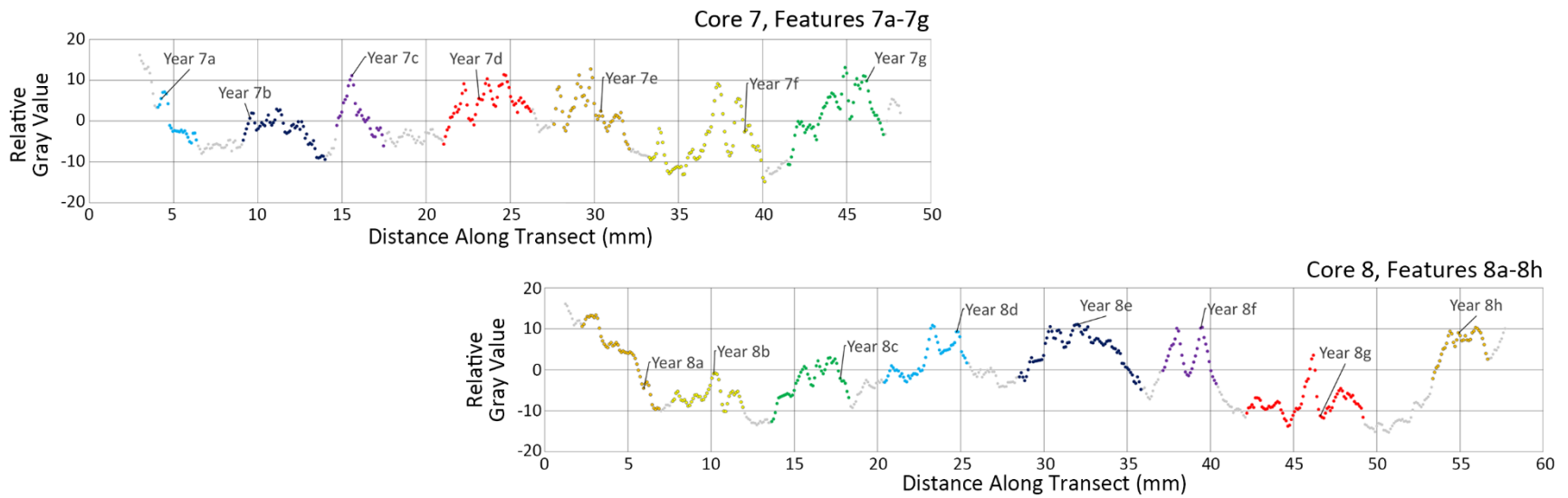


Figure 11. Detrended graphs of gray value along transects across Cores 7 and 8. Data corresponding to density features plotted in color. Year boundary associated with each feature labeled with the corresponding density feature identifier. Graphs staggered and color-coded to facilitate visual correlation of Features 7efg and 8abc.

Table 1: R-values of all possible matches of density features between adjacent cores.

Pair of Adjacent Cores	Matches of Features	Pearson's Correlation Coefficient (R)
Cores 1 and 2	1b = 2a	0.852
	1b ≠ 2b	-0.074
	1b ≠ 2c	-0.107
	1b ≠ 2d	-0.433
	1a ≠ 2a	0.645
Cores 2 and 3	2cd = 3ab	0.293
	2cd ≠ 3bc	-0.201
	2cd ≠ 3cd	-0.274
	2cd ≠ 3de	-0.082
	2ab ≠ 3ab	0.552
Cores 3 and 4	2bc ≠ 3ab	0.487
	3de = 4ab	0.805
	3de ≠ 4bc	-0.314
	3de ≠ 4cd	-0.166
	3de ≠ 4de	0.476
	3de ≠ 4ef	0.119
Cores 4 and 5	3ab ≠ 4ab	0.608
	3bc ≠ 4ab	-0.271
	3cd ≠ 4ab	-0.030
	4ef = 5ab	0.333
	4ef ≠ 5de	0.083
	4ef ≠ 5ef	0.241
	4ab ≠ 5ab	0.106
4bc ≠ 5ab	0.564	
Cores 5 and 6	4cd ≠ 5ab	0.664
	4de ≠ 5ab	-0.196
	5ef = 6bc	0.672
	5ef ≠ 6cd	0.135
	5ef ≠ 6de	0.259
	5ef ≠ 6ef	0.515
	5ef ≠ 6fg	0.746
	5ef ≠ 6gh	0.141
5ab ≠ 6bc	0.314	
Cores 6 and 7	5de ≠ 6bc	0.044
	6fgh = 7abc	0.673
	6fgh ≠ 7bcd	0.022
	6fgh ≠ 7cde	0.445
	6fgh ≠ 7def	0.405
	6fgh ≠ 7efg	0.455
	6bcd ≠ 7abc	0.651
	6cde ≠ 7abc	0.472
	6def ≠ 7abc	0.394
6efg ≠ 7abc	0.464	
Cores 7 and 8	7efg = 8abc	0.712
	7efg ≠ 8bcd	0.458
	7efg ≠ 8cde	0.271
	7efg ≠ 8def	0.083
	7efg ≠ 8efg	0.084
	7efg ≠ 8fgh	0.698
	7abc ≠ 8abc	0.361
	7bcd ≠ 8abc	0.238
	7cde ≠ 8abc	0.069
	7def ≠ 8abc	0.424
"=": Match hypothesized to be correct. "≠": Match hypothesized to be incorrect.		
Correct match of features between cores according to thin section analysis.		
Geometrically reasonable alternative match.		
Potentially geometrically illogical alternative match (included in t-tests).		
Geometrically illogical alternative match (excluded from t-tests).		

Table 2: R-values of all possible matches of pairs of density features derived from triplets of features between adjacent cores.

Pair of Adjacent Cores	Matches of Features	Pearson's Correlation Coefficient (R)
Cores 6 and 7, first pair in triplet	6fg = 7ab	0.669
	6fg ≠ 7bc	0.465
	6fg ≠ 7cd	0.316
	6fg ≠ 7de	0.262
	6fg ≠ 7ef	0.296
	6fg ≠ 7fg	-0.071
	6bc ≠ 7ab	0.532
	6cd ≠ 7ab	0.103
	6de ≠ 7ab	0.187
	6ef ≠ 7ab	0.621
6gh ≠ 7ab	0.047	
Cores 6 and 7, second pair in triplet	6gh = 7bc	0.682
	6gh ≠ 7ab	0.047
	6gh ≠ 7cd	0.243
	6gh ≠ 7de	0.203
	6gh ≠ 7ef	0.698
	6gh ≠ 7fg	0.186
	6bc ≠ 7bc	0.368
	6cd ≠ 7bc	0.714
	6de ≠ 7bc	0.515
	6ef ≠ 7bc	0.431
6fg ≠ 7bc	0.465	
Cores 7 and 8, first pair in triplet	7ef = 8ab	0.607
	7ef ≠ 8bc	0.299
	7ef ≠ 8cd	-0.045
	7ef ≠ 8de	0.266
	7ef ≠ 8ef	0.379
	7ef ≠ 8fg	0.625
	7ef ≠ 8gh	0.092
	7ab ≠ 8ab	0.266
	7bc ≠ 8ab	0.210
	7cd ≠ 8ab	-0.003
7de ≠ 8ab	0.244	
7fg ≠ 8ab	-0.292	
Cores 7 and 8, second pair in triplet	7fg = 8bc	0.641
	7fg ≠ 8ab	-0.292
	7fg ≠ 8cd	0.633
	7fg ≠ 8de	0.506
	7fg ≠ 8ef	0.134
	7fg ≠ 8fg	-0.301
	7fg ≠ 8gh	0.741
	7ab ≠ 8bc	0.022
	7bc ≠ 8bc	0.591
	7cd ≠ 8bc	0.575
7de ≠ 8bc	0.107	
7ef ≠ 8bc	0.299	
"=": Match hypothesized to be correct. "≠": Match hypothesized to be incorrect.		
Correct match of features between cores according to thin section analysis.		
Geometrically reasonable alternative match.		
Potentially geometrically illogical alternative match (included in t-tests).		
Geometrically illogical alternative match (excluded from t-tests).		